Snow thermal conductivity controls future winter carbon emissions in shrub-tundra

Johnny Rutherford[1], Nick Rutter[1], Leanne Wake[1], Alex J. Cannon[2]

[1]Department of Geography and Environmental Sciences, Northumbria University, Newcastle Upon Tyne, UK.
[2]Climate Research Division, Environment and Climate Change Canada.

Correspondence to: Johnny A. D. Rutherford (Jonathan.a.d.rutherford@northumbria.ac.uk)

Abstract

The Arctic winter is disproportionately vulnerable to climate warming and approximately 1700 Gt of carbon stored in high latitude permafrost ecosystems is at risk of degradation in the future due to enhanced microbial activity. Few studies have been directed at high-latitude cold season land-atmosphere processes and it is suggested that the contribution of winter season greenhouse gas (GHG) fluxes to the annual carbon budget may have been underestimated. Snow, acting as a thermal blanket, influences Arctic soil temperatures during winter and parameters such as snow effective thermal conductivity (K_{eff}) are not well constrained in land surface models which impacts our ability to accurately simulate wintertime soil carbon emissions. To address this, we investigated the impacts of implementing a K_{eff} parameterisation more suitable to Arctic snowpacks into the Community Land Model (CLM5.0). A point-model version of CLM5.0 forced by an ensemble of NA-CORDEX (North American Coordinated Regional Downscaling Experiment) future climate realisations (RCP 4.5 and 8.5) indicates that median winter CO_2 emissions will have more than tripled by the end of the century (2066-2096) under RCP 8.5. Implementing the refined K_{eff} parameterisation increases simulated winter CO_2 in the latter half of the century (2066-2096) by 130% and CH_4 flux by 50% under RCP 8.5 compared to the widely used default K_{eff} parameterisation. The influence of snow K_{eff} parameterisation within CLM5.0 on future simulated CO_2 and CH_4 is at least as significant, if not more so, than climate variability from a range of NA-CORDEX projections to 2100. The average difference in refined K_{eff} compared with the default K_{eff} raises minimum winter soil temperatures by 4-7 $^{\circ}$C by the end of the century under RCP 4.5 and 8.5. Furthermore, CLM5.0 simulations using the refined K_{eff} show an extension of the early winter (Sept-Oct) zero-curtain, by nearly a month under RCP 8.5. Consequently, recent increases in both zero-curtain duration and winter CO_2 emissions appear set to continue to 2100. Modelled winter soil temperatures and carbon emissions further highlight the importance of climate mitigation in preventing a significant increase in winter carbon emissions from the Arctic in the future.

1 Introduction

It is estimated that ~1700 Gt of carbon is stored in permafrost ecosystems of northern latitudes (Miner et al., 2022), which accounts for half of the global soil carbon storage (Hugelius et al., 2014), and is at risk of degradation due to climate change

(Koven et al., 2013). Near surface permafrost temperature has been increasing 1.1°C per decade since 1987 (AMAP, 2017) which acts to reduce near-surface permafrost extent and increase active layer thickness (Intergovernmental Panel on Climate, 2023); such loss of permafrost drives further release of carbon in the form of CO_2 during winter. Arctic winters are estimated to warm by 4.8°C by 2100 compared to 2.2°C in the summer over the same period (Webb et al., 2016, Christensen et al., 2013). Climate warming has enhanced the warming of soil at Arctic sites in the recent past (AMAP, 2017, Ednie and Smith, 2015) and future warming will enhance microbial decomposition of soil organic matter, driving subsequent release of carbon dioxide (CO_2) and methane (CH_4) (Natali et al., 2019, Schuur et al., 2015). Furthermore, the winter carbon flux is crucial to the annual carbon budget, as demonstrated through flux measurements from a tundra site, where approximately 60% of CO_2 uptake in the growing season was then lost in the non-growing period, and CH_4 emissions during this period accounted for 30% of the annual budget (Kittler et al., 2017). Arctic tundra ecosystems, once considered to be carbon sinks, are increasingly acting as carbon sources due to elevated winter carbon emissions driven by rising temperatures and deeper snow cover (Pongracz et al., 2021, Fahnestock et al., 1999, Welker et al., 2000, Schimel et al., 2004). Future winter emissions will likely offset growing season uptake under Representative Concentration Pathways (RCP) 4.5 (medium global emission scenario) and 8.5 (high global emission scenario) (Natali et al., 2019). Additionally, the Arctic winter is longer than the growing season (the latter being typically 2-5 months in length) , and therefore may represent a substantial input of carbon to the atmosphere that is not accurately represented in current climate models nor quantified accurately in global carbon budgets (Treat et al., 2024). Assessing simulations of heat and gas fluxes to and from subnivean soils is therefore critical in understanding how well models, such as The Community Land Model (CLM5.0; (Lawrence et al., 2019), can be expected to simulate future carbon cycling in the Arctic.

Arctic snow is a key determinant of ground temperature and plays a major role in the wider hydrological and ecological Arctic system (Callaghan et al., 2011). The hydrological cycle in the Arctic is projected to intensify throughout the 21st century and new model estimates from the Coupled Model Intercomparison Project 6 (CMIP6) support a future transition from a snow- to rain-dominated Arctic in the summer and autumn by 2100 (McCrystall et al., 2021). Despite future temperatures still being cold enough to enhance snowfall, winter rainfall also intensifies, with projected increases even matching that of snow (Bintanja and Andry, 2017). Snow is a key determinant of ground temperature and-freeze thaw state through its insulating properties (Bigalke and Walsh, 2022). The prospect of a rain dominated Arctic has implications for soil temperature, through changes in snow cover duration (Mudryk et al., 2019, Mudryk et al., 2020), insulative and structural snow properties (Cohen et al., 2015, Serreze et al., 2021), and increased soil moisture (Trenberth, 1998, Cohen et al., 2015). In the recent past (1979-2018) snowpack properties feature significant increases in spring snow bulk density (May and June), a downward trend in snow cover duration and an upward trend in wet snow, all of which result in a soil surface temperature increase of +0.41 K decade^{-1} in winter (Royer et al., 2021). Such temperature increases, induced by snowpack evolution may contribute to increased soil heterotrophic respiration and carbon release (CO_2 and CH_4) in future winters (Natali et al., 2019).

The 'shoulder' seasons, defined here as the early (after summer plant senescence has ended) and late (before snowmelt is complete) winter period (Natali et al., 2019), are a critical period in the context of the annual Arctic carbon budget, especially in terms of CH_4 where zero-curtain (when soil temperatures are poised near 0°C, such as in early winter) emissions alone contribute around ~20% of the annual budget (Zona et al., 2016). In terms of CO_2, historic early winter season emission rates have increased 73%± 11% since 1975 (October-December) (Commane et al., 2017) in response to a warming climate, demonstrating the vulnerability of this period to future warming. To date Earth System Models (ESMs) have poorly simulated respiration in the early winter shoulder season (Commane et al., 2017) which is a key component of the annual Arctic carbon budget (Kittler et al., 2017). This study addresses this knowledge gap by examining how projected changes in shoulder season air temperature, precipitation, snow thermal conductivity and soil temperature influence cold season carbon dynamics (Figures 2-5).

Land Surface Models (LSMs) such as CLM5.0 struggle to accurately reproduce cold-season CH_4 and CO_2 emissions due to uncertain numerical representation of mechanisms controlling heterotrophic respiration (Zona et al., 2016, Commane et al., 2017, Tao et al., 2021, Natali et al., 2019). One such mechanism is the mediation of winter soil temperatures by the insulating effect of seasonal snow. The default parameterisation of snow thermal conductivity (K_{eff}, W m^{-1} K^{-1}, Jordan (1991)) in CLM5.0 produces winter soil temperatures that are colder than observations (Dutch et al., 2023) which may contribute to an underestimation of soil respiration in the early winter (Commane et al., 2017). Sturm et al. (1997) presented an alternative parameterisation for K_{eff} derived from extensive Arctic snow measurements (n=488) that was implemented into CLM5.0 by Dutch et al. (2023). The Sturm et al. (1997) parameterisation is more relevant for Arctic snow types compared to Jordan (1991), as it accounts for snow layers such as basal depth hoar and wind-slab within the snowpack and produced more accurate simulations of subnivean soil temperature (Dutch et al., 2023). Further, the CLM5.0 default soil moisture threshold for decomposition (Ψ_{min} = -2) is too high to permit sub-zero soil respiration and this has been identified as a limitation in winter simulations (Tao et al., 2021, Dutch et al., 2023). Similarly, CLM5.0 default settings of Q10 (1.5) and Q10ch4 (1.3) which dictate respiratory responses to changes in temperature are too low for Arctic tundra environments (Dutch et al., 2023, Müller et al., 2015). These parameters Ψ_{min}, Q10 and Q10ch4, alongside K_{eff}, require adjustment to realistically simulate soil temperature (TSOI) respiration (SR) and methane flux (FCH4) under cold season conditions. Implementing the Sturm et al. (1997) parameterisation reduces cold bias in simulated soil temperatures by two-thirds. Further, while default CLM5.0 produces negligible winter NEE, combining the Sturm et al. (1997) parameterisation with a mid-range value for Ψ_{min} (-20) produces winter NEE values consistent with field observations (Dutch et al. 2023, Figure 5). Our study applies Q10 and Ψ_{min} values suitable for tundra soil as defined by Dutch et al. (2023) to investigate the influence of different K_{eff} parameterisations on future projections of soil temperature and carbon emissions.

This study assesses the sensitivity of SR (i.e. soil CO_2 flux to the atmosphere during winter) and CH_4 flux to K_{eff}, Ψ_{min}, Q10 and Q10ch4 within CLM5.0, and presents future projections of carbon emissions for Trail Valley Creek to 2100. Firstly, future

changes in Arctic meteorology at TVC are analysed using an ensemble (n=33) of future NA-CORDEX projections (McGinnis and Mearns, 2021), representing varying Global Climate Model-Regional Climate Model (GCM-RCM) combinations; RCP scenarios (4.5; n=6 and 8.5; n=27) and RCM resolutions (0.22 degrees; n=11, and 0.44 degrees; n=22). The NA-CORDEX ensemble is then applied to a point model of the default version CLM5.0 ('CORDEX-Jordan') to simulate present (2016-2046) and future (2066-2096) Snow Water Equivalent (SWE), 10cm Ground Temperature (GT10) and Soil Moisture (SOILLIQ) and resulting winter SR and CH_4 fluxes. The ensemble of experiments is then re-run, with the representation of K_{eff} changed from Jordan et al. (1991) to Sturm et al. (1997) to assess the impact on soil temperature; this ensemble is named 'CORDEX-Sturm'. Finally, a plausible parameter space of Ψ_{min}, Q10 and Q10ch4 for Arctic environments is applied to each experiment grouping (CORDEX-Jordan and CORDEX-Sturm) to assess the effect of assumptions governing the moisture- and temperature-related controls on soil respiration, resulting in an overall set of 396 experiments to quantify the effects of parametric and future climate uncertainty on carbon emissions at TVC.

2 Methodology

2.1 Study Location

Point scale CLM5.0 simulations are produced for Trail Valley Creek (TVC; 68° 45' N, 133° 30' W), a research basin on the boundary of the boreal-tundra ecotone ~50km north of Inuvik in the Inuvialuit Settlement Region of western Inuit Nunangat, in the Western Canadian Arctic. The basin lies within the Inuvialuit Settlement Region near the Inuvik-Tuktoyaktuk Highway. Vegetation consists of shrub tundra and is dominated by mineral earth hummocks. Mean annual air temperature from 1999-2018 averaged -7.9°C (Grünberg et al., 2019) with average seasonal variations of +10°C in summer and -25°C in winter (1995) (Marsh et al., 2002). Air temperatures increased 1.1°C per decade during the 1990-2018 period with the strongest warming observed in May (2.8°C per decade) (Grünberg et al., 2019). Snow depth at TVC is typically <50cm, with deeper packs associated with variations in topography and vegetation (King et al., 2018). Snow is often re-distributed by wind resulting in scour and snow drift features (Thompson et al., 2016). Snow cover typically lasts for 8 months (Oct-May) and underlying permafrost is between 350-500m in thickness with an active layer of 0.5-1.0m (Wilcox et al., 2019, Dutch et al., 2023). Tundra environments occupy ~31% of the Canadian Arctic (Bliss and Matveyeva, 1992, Quinton et al., 2000) and well-drained, shrub- and lichen covered uplands, such as those at TVC, comprise 80% of the Arctic-boreal region (Voigt et al., 2023). TVC has long lasting concurrent hydrometeorological and Eddy Covariance (EC) carbon flux data since 2013 (Tutton, 2024) which can be used to bias correct future meteorological simulations (see section 2.2).

2.2 Meteorological forcing data and simulations using CLM5.0

NA-CORDEX meteorological forcing data (incoming shortwave and longwave radiation, precipitation, humidity, wind speed, air pressure, min and max temperature) for the grid cell closest to TVC provides CLM5.0 with daily meteorological conditions to 2100. This forcing dataset was generated from a suite of 33 bias-corrected GCM-RCM combinations for North America

(McGinnis and Mearns, 2021) ran under full transient conditions with a historical period spanning 1950-2005 and with scenarios RCPs 4.5 and 8.5 for 2006-2100 at 0.22 and 0.44 degree resolution. To minimise the influence of climate model bias on model results, meteorological forcing data from the climate models were bias-adjusted to match statistical characteristics of meteorological observations (Tutton, 2024) in the overlapping 1992-2022 period following Cannon (2018) and Cannon et al. (2022). CLM5.0 was run in "point mode" (a 0.1° x 0.1° grid cell) and centred at the location of TVC as per Dutch et al. (2021). Model spin up is required to stabilise carbon pools within CLM5.0 prior to model initiation; model simulations were spun-up for 512 years and full details of these spin-up conditions are outlined in Dutch et al. (2023).

2.3 CLM5.0 parameter assessment

K_{eff} describes the rate of heat transfer from the atmosphere through the snow to underlying soils and as such K_{eff} influences heterotrophic respiration rates and subsequent production of CO_2 and CH_4. CLM5.0 default K_{eff} parameterisation using Jordan *et al.* 1991 overestimates K_{eff} by a factor of 3 for tundra snow (Dutch et al., 2021). In CLM5.0, K_{eff} is parameterised as a function of snow density (ρ, kg m^{-3}) (equation 1), which is calculated from relative proportions of ice mass (m_i) and liquid water mass (m_{lw}), weighted by the snow cover fraction (F_{sno}) multiplied by the height of the snow layer (h_{sl}) for each grid cell. K_{eff} can then by calculated using coefficients in equation 2 (Jordan *et al.* 1991 which utilises the thermal conductivity of air and ice ($K_{ice} - K_{air}$), or equation 3 (Sturm *et al.* 1997):

$$\rho = \frac{m_i \times m_{lw}}{F_{sno} \times h_{sl}} \quad (1)$$

$$K_{eff} = K_{air} + (((7.75 \times 10^{-5} \times \rho) + (1.105 \times 10^{-6} \times \rho^2))(K_{ice} - K_{air})) \quad (2)$$

$$\begin{cases} K_{eff} = 0.138 - 1.01\rho + 3.233\rho^2, & 0.156 \leq \rho \leq 0.6 \\ K_{eff} = 0.023 + 0.234\rho, & \rho < 0.156 \end{cases} \quad (3)$$

The use of the snow thermal conductivity parameterisation following Sturm et al. (1997) improved soil temperature simulations in CLM5.0 at TVC (Dutch et al., 2021) and at other sites with additional land surface models (Royer et al., 2021). Here, the Sturm et al. (1997) K_{eff} parameterisation was applied to future CLM5.0 simulations and compared with the default parameterisation which follows Jordan (1991). CLM5.0 uses Ψ_{min} to describe the soil moisture threshold for respiration (MPa). Without adjustments to Ψ_{min}, CLM5.0 simulates near-zero soil respiration for the majority of the snow-covered non-growing season which is not consistent with field observations (Dutch et al., 2023). Reducing Ψ_{min} facilitates respiration in moisture-limited soils (Tao et al., 2021). Ψ_{min} is applied in CLM5.0 as described by Andren and Paustian (1987):

$$r_W = \sum_{j=1}^{5} \begin{cases} 0 & \text{for } \Psi_j < \Psi_{min} \\ \frac{log(\Psi_{min}/\Psi_j)}{log(\Psi_{min}/\Psi_{max})} w_{soil,j} & \text{for } \Psi_{min} < \Psi_j < \Psi_{max} \\ 1 & \text{for } \Psi_j > \Psi_{max} \end{cases} \quad (4)$$

where the rate scalar for soil water potential (r_W) is calculated from Ψ_j that is the soil water potential in soil layer j, and Ψ_{min}/Ψ_{max} as upper and lower limits. The default values of Ψ_{min}/Ψ_{max} for CLM5.0 are -2 MPa and -0.002 MPa respectively. As well as K_{eff} and Ψ_{min}, we also focus on the temperature soil decomposition modifier r_T which is parameterised using a Q10 function which describes the dependence of biological metabolic processes, such as respiration, on temperature. r_T is calculated as follows:

$$r_T = Q_{10}^{(\frac{T_j - T_{ref}}{10})} \quad (5)$$

Where T_j is the temperature of soil layer j and T_{ref} is a reference temperature with a default value of 25°C. CLM5.0 uses a fixed Q10 of 1.5, however, this is unrealistic for Arctic ecosystems which typically have an average Q10 of 5.4 (Chen et al., 2020). A range of Ψ_{min} ('minpsi_hr', -2 to -20) and Q10 ('q10_hr', 'froz_q10', 1.5 to 7.5) was used to assess the sensitivity of CLM5.0 for future simulations to 2100. A parameter 'q10ch4' within the methane module of CLM5.0 which controls temperature dependency of methane production is available and was tested from its default value 1.33 to a plausible extreme of 4 (Müller et al., 2015, Riley et al., 2011) with a reference temperature of 22°C. We implemented a broad range of Q10 and q10ch4 (1.5 – 7.5) to capture variability in the temperature sensitivity of soil respiration associated with differences in carbon pool lability (Fierer et al., 2005, Yan et al., 2017). The full range of tested parameters are presented in Fig. A1.

A major focus of this study is the winter season when snow is on the ground (i.e. the snow-covered non-growing season). We define this period as the time when all model ensemble members (RCP 4.5 n=6, RCP 8.5 n=27) agree that SWE is >5mm. Simulations of SR and FCH4 are filtered by these constraints so the analysis in Figures 5 and 6 is focused only on carbon fluxes across a common snow-covered, non-growing season in all scenarios and forcing datasets. The resulting data is therefore weighted towards a shorter snow-cover period as ensemble members capture a range of snow-cover durations. Periods of the winter season that are critical to driving the timing and rates of respiration are described as follows. The 'zero-curtain period' is defined as days where soil temperature falls between -0.75 and 0.75°C (Tao et al., 2021, Zona et al., 2016) while 'shoulder seasons' describes annual transitional periods of snow melt (Apr-May) and plant senescence-to-freeze up (Sep-Oct) (Shogren et al., 2020). Testing for statistically significant differences between distributions of future meteorological conditions and median winter carbon fluxes are evaluated using the non-parametric Kolmogorov–Smirnov (K-S test) test.

3 Results

3.1 NA-CORDEX meteorological forcing data

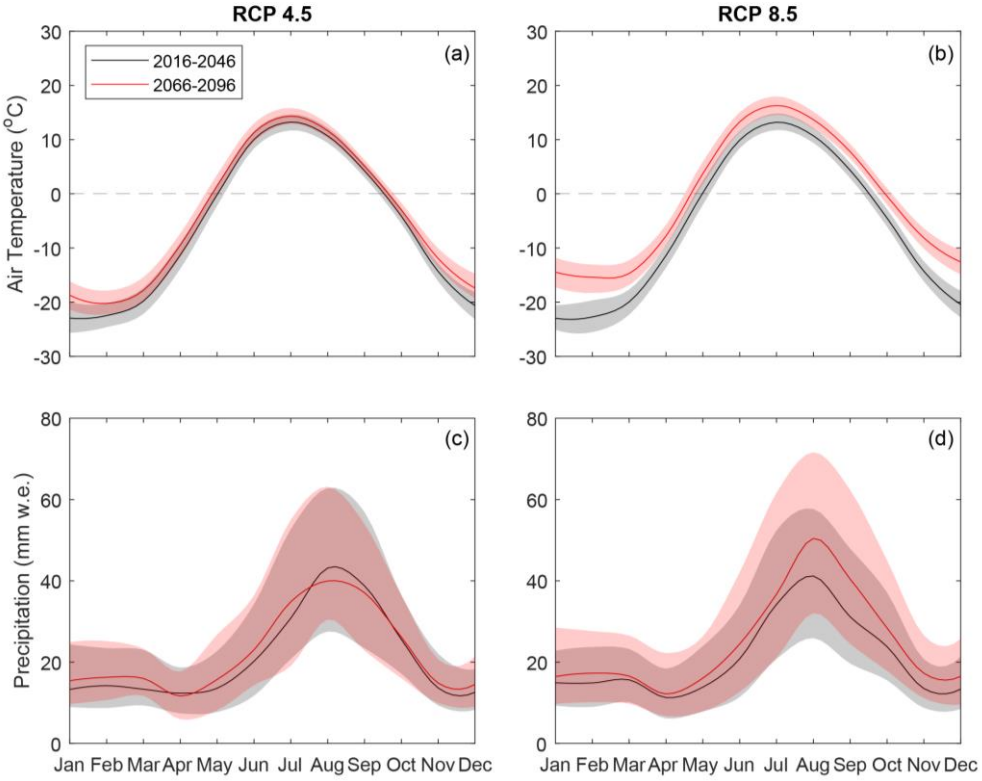

Figure 1 – Simulated median monthly precipitation and temperature over two 30-year time periods: 2016-2046 (black) and 2066-2096 (red) under RCP 4.5 and RCP 8.5, for TVC using meteorological data from an ensemble of 33 NA-CORDEX GCM-RCM combinations (RCP 4.5 n=6, RCP 8.5 n=27). Shaded areas represent the 25th and 75th percentiles (variability between individual ensemble members for precipitation is presented in Appendix A1).

Bias-corrected NA-CORDEX model ensemble projections show an increase in future winter air temperatures at TVC, which intensifies under RCP 8.5, with a 9°C increase from present to future in median January air temperatures (Figure 1a and b). The timing and rate of air temperature increase in the spring is comparable between present and future, whereas the rate of cooling after the summer maximum decreases in the future under RCP 8.5 (a decrease of 6.8°C/month in the present and 5.7°C /month in the future for Jul-Dec). Under RCP 8.5, significant increases in precipitation are projected from Jul-Dec, the largest increase occurring in August from 41 to 50 mm w.e. (Two sample K-S test, test statistic: $D=0.16$, $p<0.05$, Figure 1d). In shoulder season months (April, May, September and October), projected air temperatures increase on average by 1.6°C under RCP 4.5 and 3.7°C under RCP 8.5. Warmer future air temperatures influence the phase of future precipitation with more precipitation falling as rain than snow, especially in transitional shoulder seasons between summer and winter (Figure 2).

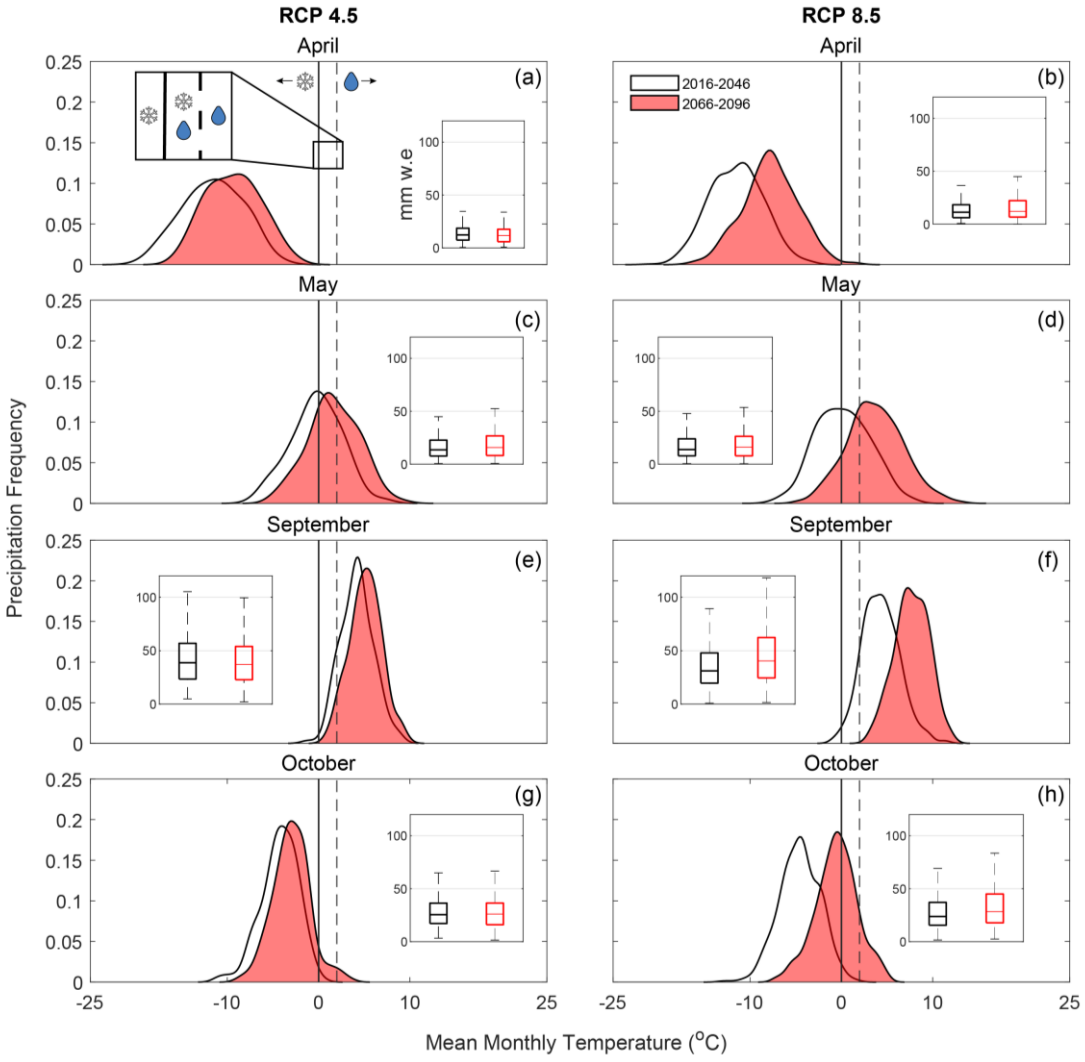

Figure 2 – Half-violin plots show the frequency distribution of precipitation events as a function of air temperature for TVC in April, May, September and October under RCP 4.5 (left) and RCP 8.5 (right). from an ensemble of 33 NA-CORDEX GCM-GCM combinations (RCP 4.5 n=6, RCP 8.5 n=27). The white violins with black outlines represent 2016-2046 and red violins 2066-2096. The height of each violin represents the frequency of precipitation events at a given temperature. The solid and dashed black lines at 0 and 2 ˚C show transitional temperatures between snow and rain where CLM5.0 treats the transition in precipitation phase as a linear ramp. Inset boxplots show monthly total precipitation for the two 30-year periods.

Changes in air temperature in May and October cause a phase shift (snow to rain) in total monthly precipitation under RCP 8.5 from present to future (Figure 2, d and h). In May, in the present (2016-2046) 50% of precipitation events in the current period fall within 0-20˚C (as rain, or as a mix of snow and rain) compared to 87% in the future (2066-2096). In October, only 2% of precipitation events fall within 0-20˚C compared to 40% in the future. Furthermore, in May, future (red) peak precipitation frequency occurs at 2.7˚C compared to -0.6˚C at present (black), and in October at -0.5˚C compared to -4.6˚C at

present (Figure 2) under RCP 8.5 which indicates a shoulder season precipitation shift from majority snow to a mix of rain/snow. By contrast, differences between current and future total precipitation are small (Figure 2, a-h, insets), and increases from present to future are significant only in September (Two sample K-S test: 31 to 40mm, $D=0.17$, $p<0.05$) and October (Two sample K-S test: 23 to 28mm, $D=0.12$, $p<0.05$) under RCP 8.5. As such, changes in magnitude and phase of precipitation in the shoulder seasons may influence future snow-season length, snow thermal conductivity (due to an increase in melt conditions) and subsequent temperature and moisture of soils.

3.2 CLM5.0 simulations

3.2.1 Environmental conditions

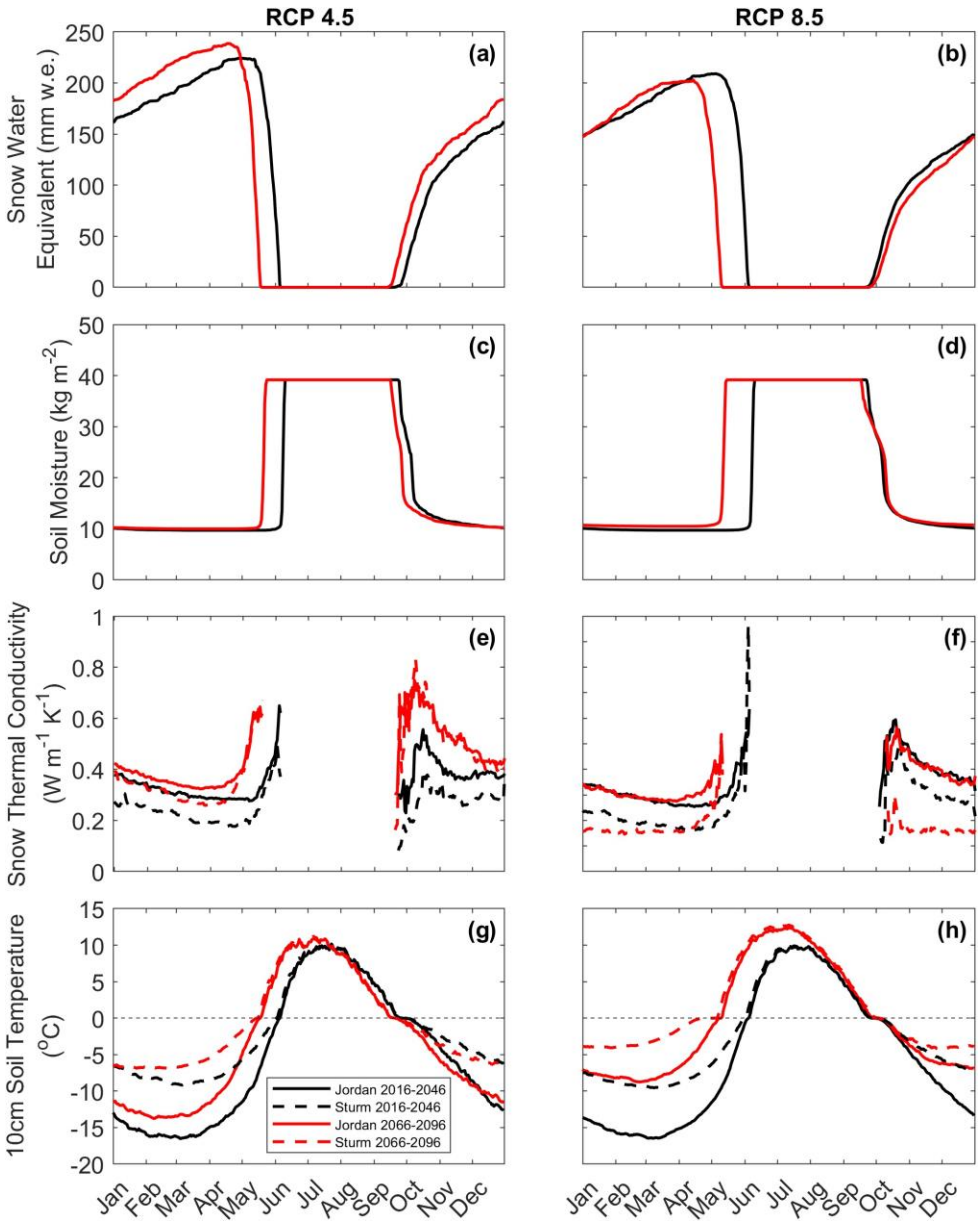

Figure 3 – CLM5.0 simulated median daily snow water equivalent (SWE; a,b), , soil liquid water (12cm) content (c,d) snow thermal conductivity (e,f) and 10cm soil temperature (g,h) over two 30-year time periods: 2016-2046 (black) and 2066-2096 (red) under RCP 4.5 and RCP 8.5, for TVC using input meteorological data from an ensemble of 33 RCM-GCM combinations (RCP 4.5 n=6, RCP 8.5 n=27). Solid and dashed lines show ensemble median values for CORDEX-Jordan and CORDEX-Sturm experiments respectively.

An increase in future rainfall in September impacts both the timing of winter onset of snow accumulation and the magnitude of peak SWE later in the winter (Figure 3). The duration of winter snow cover is shorter in the future where future spring melt-out occurs between 18 to 25 days earlier in both RCP scenarios, while the timing of initial snow accumulation remains similar (+/- 4-6 days). Projected future peak annual SWE shows an increase of 14 mm w.e. under RCP 4.5 and a decrease of 6 mm w.e. under RCP 8.5 and early spring snow melt is coincident with earlier increases in soil temperature in mid-late spring (Figure 3, a-d). Compared to CORDEX-Jordan, Snow thermal conductivity using CORDEX-Sturm is lower on average by 0.07 and 0.14 W m^{-1} K^{-1} under RCP 4.5 and RCP 8.5 respectively.

Using CORDEX-Sturm, the median minimum winter soil temperature is 4-7˚C warmer by the end of the century (2066-2096) compared to CORDEX-Jordan under both RCP scenarios (Figure 3,g,h). Warmer air temperatures predicted for the end of this century (Figure 1, a,b) will warm the soil, and snow cover will then insulate the soil from the colder atmosphere, maintaining these elevated soil temperatures throughout the winter (Figure 3,g,h).

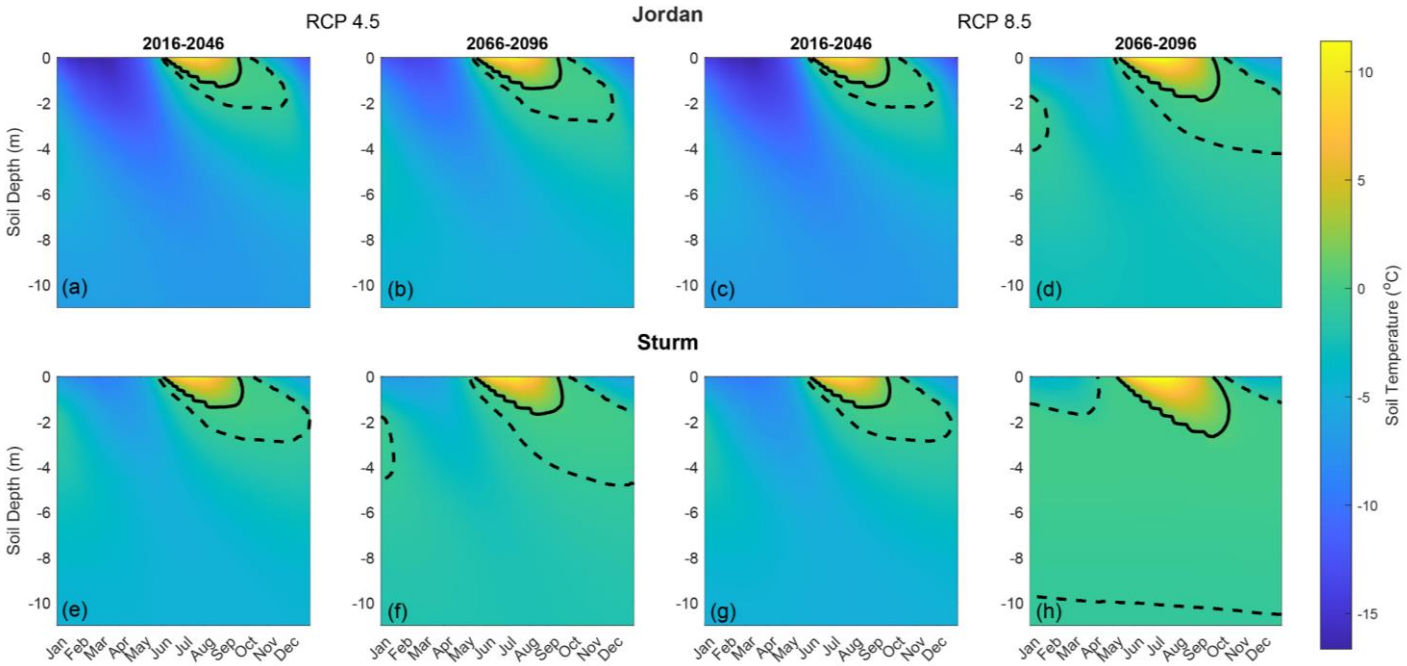

Figure 4 – CLM5.0 simulated median daily soil temperature with depth over two 30-year time periods: 2016-2046 and 2066-2096 under RCP 4.5 (left) and 8.5 (right). 1st row plots show CLM5.0 under default K_{eff} parameters (Jordan et al. 1991) and 2nd row plots show an alternative parameterization for snow thermal conductivity (Sturm et al. 1997). Solid black lines indicate 0.75˚C and dashed -0.75˚C, indicating zero curtain between them.

Due to earlier snow melt, soils are predicted to thaw earlier in the year under both RCP scenarios (RCP 4.5 = 19 days, RCP 8.5 = 26 days; Figure 3, e, f). The timing of soil moisture increase in May and June remains similar in the present (2016-2046) between RCP 4.5 and 8.5 but occurs 20-30 days earlier in the future (2046-2096). By comparison, the timing of soil moisture decrease in September and October remain similar at Julian day 257-267 between the two RCP scenarios and 30-year time

periods. Modelled soil moisture plateaus at 10 kg m^{-2} from October-May and reaches saturation 39.167 kg m^{-2} from late May-early October.

Evidence of a late winter (February-March) zero-curtain period is minimal across all but one scenario (Figure 4h), however soil temperatures at depths up to 10m suggest that the zero-curtain duration from Aug-Dec increases by 10 and 36 days in the future under CORDEX-Jordan and CORDEX-Sturm respectively (Appendix B1). In the future under RCP 8.5, autumn shoulder season (Sep-Oct) near-zero temperatures penetrate up to 6m deeper into the soil column compared with the present day in the CORDEX-Sturm simulations (Figure 4h). An earlier spring snow melt, increasing winter soil temperatures, and longer zero-curtain duration combine to create the conditions for increased cumulative seasonal carbon emissions in the future at TVC.

3.2.2 CO_2 and CH_4 emissions

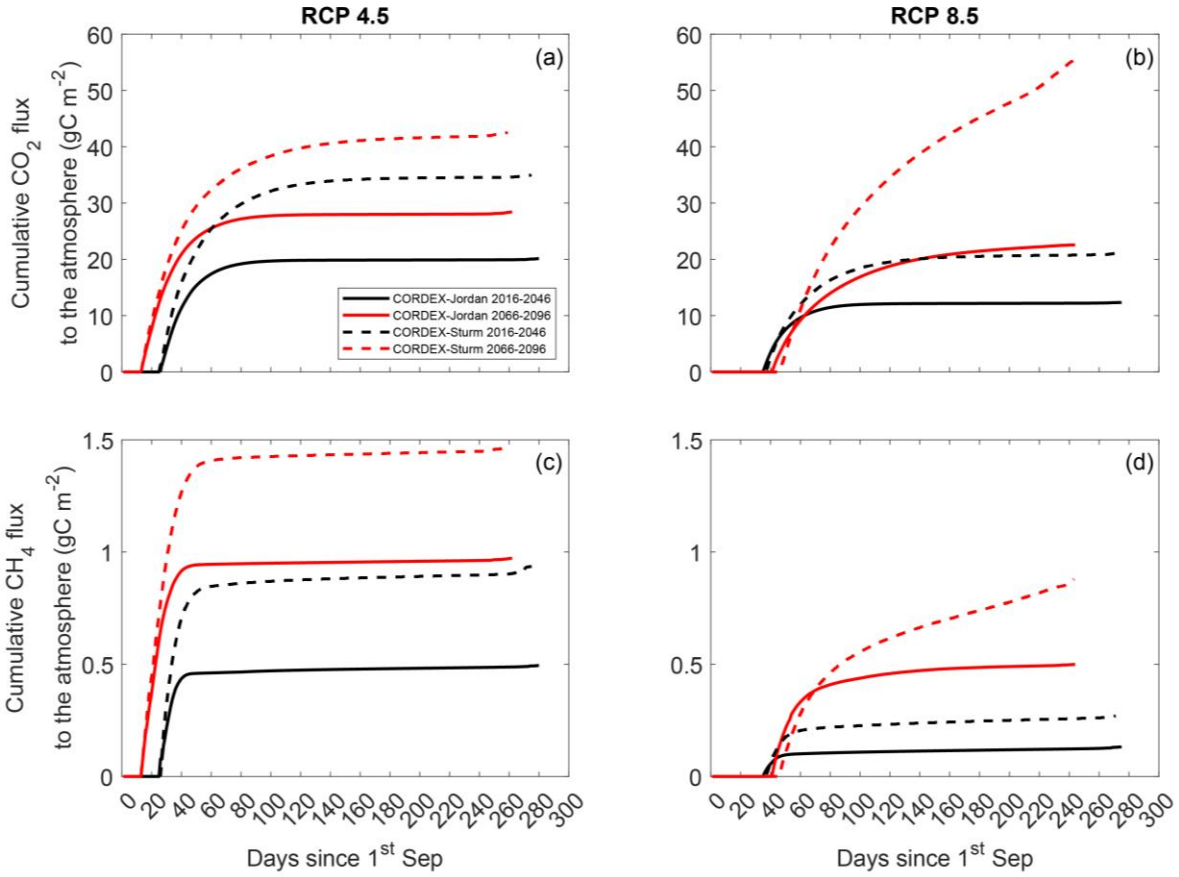

Figure 5 – CLM5.0 simulated cumulative CO_2 and CH_4 flux to the atmosphere during snow-cover periods over two 30-year time periods: 2016-2046 (black) and 2066-2096 (red) under RCP 4.5 and RCP 8.5, for TVC using meteorological forcing from an ensemble of 33 RCM-GCM combinations (RC P 4.5 n=6, RCP 8.5 n=27). Solid lines show median values from CORDEX-Jordan ensemble and dashed lines show values for the CORDEX-Sturm ensemble. Variable plot line lengths are indicative of changes in snow-season length.

Cumulative snow-covered CO_2 and CH_4 fluxes are projected to increase under both RCP scenarios (Figure 5) with the highest CO_2 increase produced for CORDEX-Sturm (34.2 g CO_2 m^{-2}; from 21.1 to 55.3 gCO_2 m^{-2}) under RCP 8.5. An earlier onset of snow in 2066-2096 facilitates earlier emissions of CO_2 and CH_4 during the Autumn under RCP 4.5 (12-13 days post Sept 1st; Figure 5, a, c) compared with RCP 8.5 (41-47 days post Sept 1st; Figure 5, b, d). Delayed snow onset reduces overall cumulative carbon emissions during the snow-cover period under RCP 8.5 (Figure 5, b, d) compared with RCP 4.5 (Figure 5, a, c). By the start of November, cumulative CO_2 emissions have reached 50-90% of their winter totals, highlighting the importance of autumn shoulder season emissions to the winter CO_2 budget. Under RCP 4.5 there is minimal increase in cumulative CO_2 after mid-late November (after day 80) with increases of 0.02 gCO_2 m^{-2} day^{-1} and 0.00015 gCH_4 m^{-2} day^{-1}. Comparatively, under RCP 8.5, higher levels of emissions continue deeper into the winter with average increases of 0.07 gCO_2 m^{-2} day^{-1} and 0.003 gCH_4 m^{-2} day^{-1} (day 80 to day 240) (Figure 5). Applying the Sturm et al. (1997) snow thermal conductivity scheme within CLM5.0 increases the total accumulation of winter CO_2 at TVC from 2016-2100 by 50-150% and CH_4 by 50-74% across both RCP scenarios compared to CORDEX-Jordan. Appendix D1 presents a comparison between cumulative emissions limited to when snow is on the ground as per Figure 5 and those unconstrained by snow cover. The cumulative emissions not limited to the snow-covered period are 3-4 times higher than those constrained by snow and highlight the impact of the early winter period on accumulated winter soil carbon emissions.

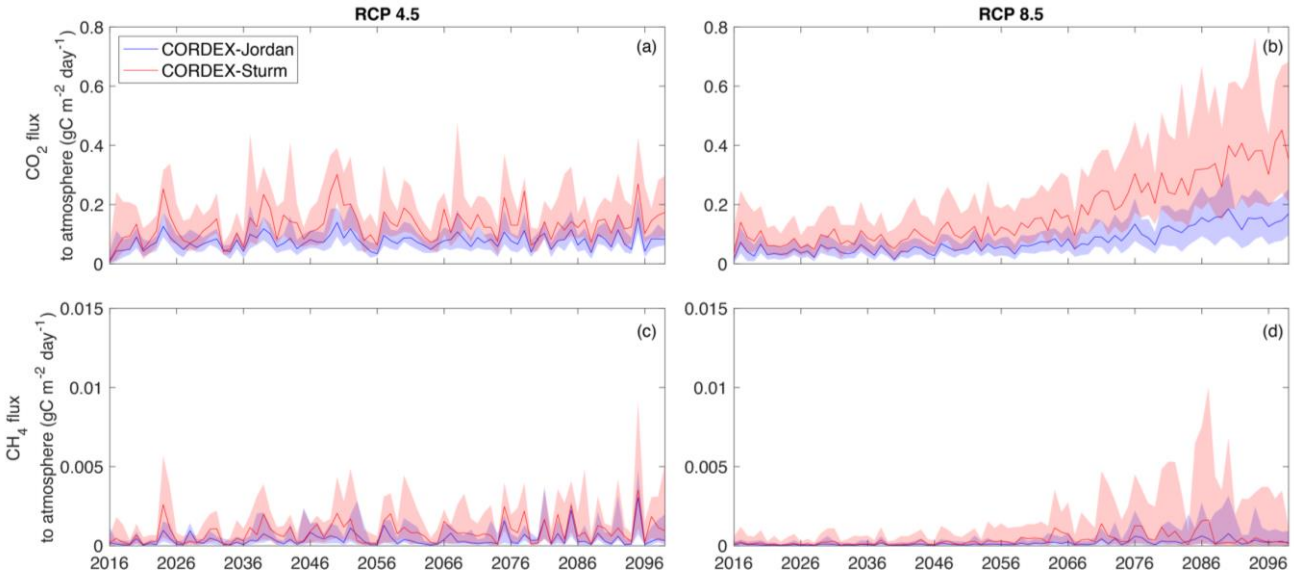

Figure 6 – CLM5.0 simulated median soil respiration for the winter season, comparing the CORDEX-Jordan ensemble with CORDEX-Sturm for two RCP scenarios (RCP 4.5 n=6, RCP 8.5 n=27). Shaded areas represent 75th and 25th percentiles and represent the ensemble distribution. Ensemble median and uncertainty calculations incorporate a range of Ψ_{min}, Q10 and Q10ch4 (Appendix E1).

From 2016-2046 to 2066-2096, median winter CO_2 flux increases by 18% (0.11 – 0.13 gCO_2 m^{-2} day^{-1}) under RCP 4.5 and more than triples (0.08 to 0.3 gCO_2 m^{-2} day^{-1}) under RCP 8.5, using CORDEX-Sturm. CORDEX-Sturm significantly increases

winter CO_2 emissions compared with CORDEX-Jordan, by 57% (2016-2046) to 62% (2066-2096) in RCP 4.5 and 100% (2016-2046) to 130% (2066-2096) in RCP 8.5 (Two sample K-S test: D=0.26, p<0.01, Figure 6). Likewise, under RCP 8.5 CORDEX-Sturm significantly increases median CH_4 emissions by 50% during 2066-2096 compared to CORDEX-Jordan (2.5e-04 to 3.8e-04 $gCH_4\ m^{-2}\ day^{-1}$) (Two sample K-S test: D=0.13, p<0.01, Figure 6) further showing the impact of snow representation on the simulation of CH_4 from Arctic soils. Between RCP 4.5 and 8.5 median CO_2 emissions more than double (0.13 to 0.30 $gCO_2\ m^{-2}\ day^{-1}$) for the last 30 years of the century using CORDEX-Sturm. Simulations with reduced Ψ_{min} and (-20) consistently stimulate higher carbon fluxes under RCP 4.5 and 8.5 compared to simulations using the default Ψ_{min} value (-2) (Appendix E1). This is particularly evident under CORDEX-Sturm which shows average increases of 0.13-0.16 $gCO_2\ m^{-2}\ day^{-1}$ and 0.0014-0.0018 $gCH_4\ m^{-2}\ day^{-1}$ from 2016-2100. CLM5.0 simulations indicate that warmer soil conditions induced by climate warming under RCP 8.5 intensify winter carbon emissions from TVC soils in the future.

4 Discussion

4.1 Future temperature, precipitation, and snow cover

NA-CORDEX forecasts suggest rising future winter air temperatures (Figure 1) which may increase winter soil heterotrophic respiration and contribute significantly to winter carbon emissions offsetting growing season carbon uptake in the future (Natali et al., 2019, Commane et al., 2017). Mobilisation of "legacy" carbon (Pedron et al., 2023) within Arctic permafrost is of concern in a warming climate (Schuur et al., 2015) and warmer winters will enhance future climate change through carbon output from decomposition of soil carbon. Understanding changes in future Arctic air temperature and meteorology is key in determining the influence of a warming world on Arctic winter carbon emissions and vice versa.

NA-CORDEX ensemble simulations demonstrate a shift from a snow- to rain-dominated Arctic in the future, reported elsewhere in the literature (McCrystall et al., 2021) which is intensified under RCP 8.5 (Figure 2). The shift in precipitation phase in September and October will lead to a change in snow properties, particularly the effective conductivity of the snowpack. Additionally, melt conditions and rain-on-snow events in the initial stage of the snow cover season provide energy for melt through condensation of water vapour onto the snowpack (Harr, 1981, Mazurkiewicz et al., 2008). An increase in precipitation fraction falling as rain is therefore a likely driver of earlier snowmelt in CLM5.0 simulations (Figure 3). Future changes in precipitation have key, yet uncertain, implications for the Arctic surface and soil energy balance with regard to snow cover depth, timing and duration which are major factors controlling temperature variability in the upper 3 m soil (Callaghan et al., 2011).

4.2 Future soil carbon emissions

The CLM5.0 parameterisations for K_{eff}, Q10 and Ψ_{min} explored by Dutch et al. (2023) were found to be highly suitable for representing winter soil temperatures and carbon fluxes under present day conditions. This alignment between observations and simulations provides confidence in the model's ability to simulate future Arctic soil processes through to 2100. Our

simulations show that by the end of the century (2066-2096), CLM5.0 simulated median winter soil CO_2 emissions under RCP 4.5 are predicted to be less than half of those under RCP 8.5, showing that projected winter carbon emissions are tied to magnitude of global temperature increase. Winter snow cover has a significant influence on the ground thermal regime (Zhang, 2005) and it's representation within ESMs is critical for simulated soil temperatures. The more realistic K_{eff} parameterisation in the CORDEX-Sturm simulations results in reduced soil temperature biases in CLM5.0 (Dutch et al., 2023) and elevates simulated winter soil temperatures to between -10 and 0°C. Within this range, respiration rates begin to increase rapidly (Natali et al., 2019). Cumulative winter CO_2 simulations (Figure 5) under present day conditions are in line with contemporary (2016-2019) NEE simulations, generated using in-situ meteorological data at TVC Dutch et al. (2023) for both Jordan (~15-35 gCO_2 m^{-2}) and Sturm (~25-55 gCO_2 m^{-2}) parameterisations. Under RCP 8.5 cumulative winter carbon emissions from soils at TVC are projected to increase in the future despite a reduction in snow-cover duration. A reduced K_{eff} (0.07-0.14 W m^{-1} K^{-1}), as introduced by CORDEX-Sturm (Figure 3), increases cumulative winter CO_2 and CH_4 emissions from 2016-2100 by 50-150% compared with CORDEX-Jordan under both RCP 4.5 and 8.5. Natali et al. (2019) estimated that winter CO_2 emissions would increase by 41% by 2100 (from 'present', i.e. 2003-2017 conditions; Natali et al. (2019); this study 2016-2046) under RCP 8.5 whereas CLM5.0 simulations of CO_2 emissions under CORDEX-Sturm more than triple under RCP 8.5 which demonstrates the impact of snow representation on simulated soil carbon emissions. Under RCP 8.5 the magnitude of the influence of CORDEX-Sturm on winter carbon fluxes is comparable to the uncertainty in the future climate, reinforcing the importance of snow representation in future projections of Arctic carbon fluxes. The response of carbon fluxes from permafrost zones is highly sensitive to hydrological change and an increase in CO_2 emissions post-2050 (Figure 6) is indicative of soil drying where, as temperatures increases, soil CH_4 production is strongly suppressed (Lawrence et al., 2015). Soil moisture and temperature are critical controls of soil carbon emissions and adjustments to Ψ_{min}, Q10 and Q10ch4 bring CLM5.0 simulations into closer alignment with field measurements (Dutch et al., 2023). Future CO_2 and CH_4 emissions show greater seasonal variability under CORDEX-Sturm compared with CORDEX-Jordan, particularly under RCP 8.5, which suggests that soil moisture and thermal dynamics are more sensitive to snow cover in the CORDEX-Sturm configuration (Appendix E1). Further, the difference in CO_2 output between RCP 4.5 and 8.5 shows the possible impacts of climate mitigation efforts on future Arctic winter carbon emissions (Figure 6).The zero-curtain is an important period for facilitating cold season emissions from tundra ecosystems (Tao et al., 2021) and an increasing proportion of the soil at or around 0°C presents a risk of elevated carbon emissions from Arctic soils in the future. The seasonality of soil temperature is critical in controlling winter CO_2 emissions from soils, particularly the length of time at which soil remains at or near 0°C at the beginning of winter (Schimel et al., 2006). Persistent carbon emissions throughout the winter period are partly attributable to a permanently unfrozen active soil layer (Zona et al., 2016) and its influence in the future will be intensified by a longer zero-curtain period. Simulations performed in this study indicate an increase in both the duration and depth of the early winter zero curtain under future climate conditions (Figure 4). Under CORDEX-Sturm, the projected early winter zero curtain extends up to 26 days longer and reaches depths up to 6m deeper than under CORDEX-Jordan further highlighting the impact of snow representation on simulated soil temperatures. Increases in the duration of the zero-curtain is concurrent with measured borehole data from 2006-2015 at an

Arctic tundra site, which show an increase of up to 20 days, with large emissions of CO_2 between September and December in years with a longer zero-curtain period (Euskirchen et al., 2017, Larson et al., 2021). A deeper active layer (Aalto et al., 2018) and an increase in unfrozen soil (Schaefer and Jafarov, 2015, Natali et al., 2019, Elberling and Brandt, 2003) as a result of a longer and deeper zero-curtain will increase soil respiration (SR) in the future. In the recent past (1950 to 2017), both zero-curtain and cold season CO_2 emissions have increased, for one site of 0.17 and 0.36 gC m^{-2} yr^{-1} at Atqasuk, Alaska (Tao et al., 2021), and CLM5.0 simulations suggest that this is set to continue to 2100. Such increases in soil temperature and zero-curtain duration demonstrates both the influence of snow on soil temperatures at depth and the risks of climate warming on permafrost degradation and possible mobilisation of legacy carbon from Arctic soils.

Future changes in shoulder season air temperature, soil moisture, and snow cover control both CO_2 and CH_4 due to moisture limitation, oxygen limitation and soil temperature. A major fraction of cold-season CH_4 emissions occur in the early winter shoulder season, particularly the zero-curtain (Zona et al., 2016) and interannual variability in both CO_2 and CH_4 depends largely on this period (Kittler et al., 2017). Soil moisture fluctuations (Figure 3) critically impact rates of microbial decomposition of organic matter via methanogenesis which favours wet, anoxic environments. CH_4 emissions are closely tied to soil moisture in the upper 30cm of soil and are closely correlated with soil moisture fluctuations during the soil freeze-in period (Sturtevant et al., 2011). In the early winter (Sep-Oct) the soil profile is saturated which drives anoxic conditions favoured by methanogens, which increases with depth (Arndt et al., 2020). Soil moisture increases in late September between RCP 4.5 and 8.5 (Figure 3) resulting in wetter soil, alongside increased zero-curtain period at depth (Figure 4) under RCP 8.5 present a risk of increased CH_4 emissions during this early winter period in the future at TVC. Such soil moisture increases, by slowing the soil freezing process have implications for the extension of elevated CH_4 emissions longer into the winter season (Sturtevant et al., 2012). Understanding the potential impacts of climate warming on both the early and late winter shoulder seasons is therefore key for assessing the risk of elevated winter carbon emissions from tundra soils. As well as persistent winter carbon emissions, 'pulses' of CO_2 and CH_4 have been observed during both the early and late winter shoulder seasons (Raz-Yaseef et al., 2017, Mastepanov et al., 2013) where trapped gasses are released as soils fluctuate between freeze and thaw. Soil emission pulses, which are not able to be simulated by CLM 5.0, are enhanced by an increase in rain-on-snow events. Such events accelerate soil warming in spring and soils are more susceptible to cracking and rapid gas release (Raz-Yaseef et al., 2017). A shift towards a rain dominated Arctic (Figure 2) may therefore increase the abundance of spring gas pulses from soils in both frequency and distribution, increasing cumulative carbon emissions annually. Further work is required to better understand the impact of these pulses on annual carbon budgets and their representation within LSMs.

5 Conclusions

Warming air and soil temperatures are facilitating higher rates of heterotrophic respiration in CLM5.0 simulations for TVC soils, resulting in an expected increase in winter carbon output in the future under RCP scenarios 4.5 and 8.5. Such winter

emissions outpace those modelled by Natali et al. (2019) and therefore reinforce the vulnerability of Arctic soils and the carbon stored within to climate warming.

Soil temperature simulations show a lengthening of the zero-curtain period in the future as well as deeper penetration of near-zero temperatures into the soil column which will mobilise legacy carbon in the future. A longer zero-curtain period, leading to a persistently unfrozen active layer of soil where higher rates of soil respiration persist for longer into the snow-cover period, poses a risk of significantly increased cumulative carbon output in the future from tundra soils.

Modelled winter carbon emissions demonstrate the importance of climate mitigation in preventing a significant increase in the Arctic winter carbon budget. Use of parameterisation for K_{eff} from Sturm et al. (1997) reduces soil temperature biases and presents significantly higher CO_2 production from 2016-2100 compared to default parameters from Jordan (1991). An improved representation of K_{eff} exacerbates already increasing CO_2 emissions from Arctic tundra caused by a warming climate and the influence of the selected K_{eff} parameterisation is shown to be as important, if not more, as the variability in future climate on simulated carbon emissions from Arctic tundra. Projected CO_2 and CH_4 emissions are highly sensitive to parameters K_{eff}, Ψ_{min}, Q10 and Q10ch4 which govern soil respiration. We find that lower Ψ_{min} consistently increases cold season carbon fluxes and higher Q10 suppressed them, which aligns with the findings of Dutch et al. (2023). Implementing the Sturm et al. (1997) K_{eff} parameterisation increased the sensitivity of modelled carbon emissions to Ψ_{min} and Q10 compared with the default K_{eff} parameterisation. Further work should aim to improve representations of snow thermal conductivity in LSMs while increasing the spatial coverage of future simulations to allow a more holistic outlook for Arctic soil carbon emissions and better inform climate mitigation strategies and carbon budgets.

Appendices

APPENDIX A - NA-CORDEX future meteorology

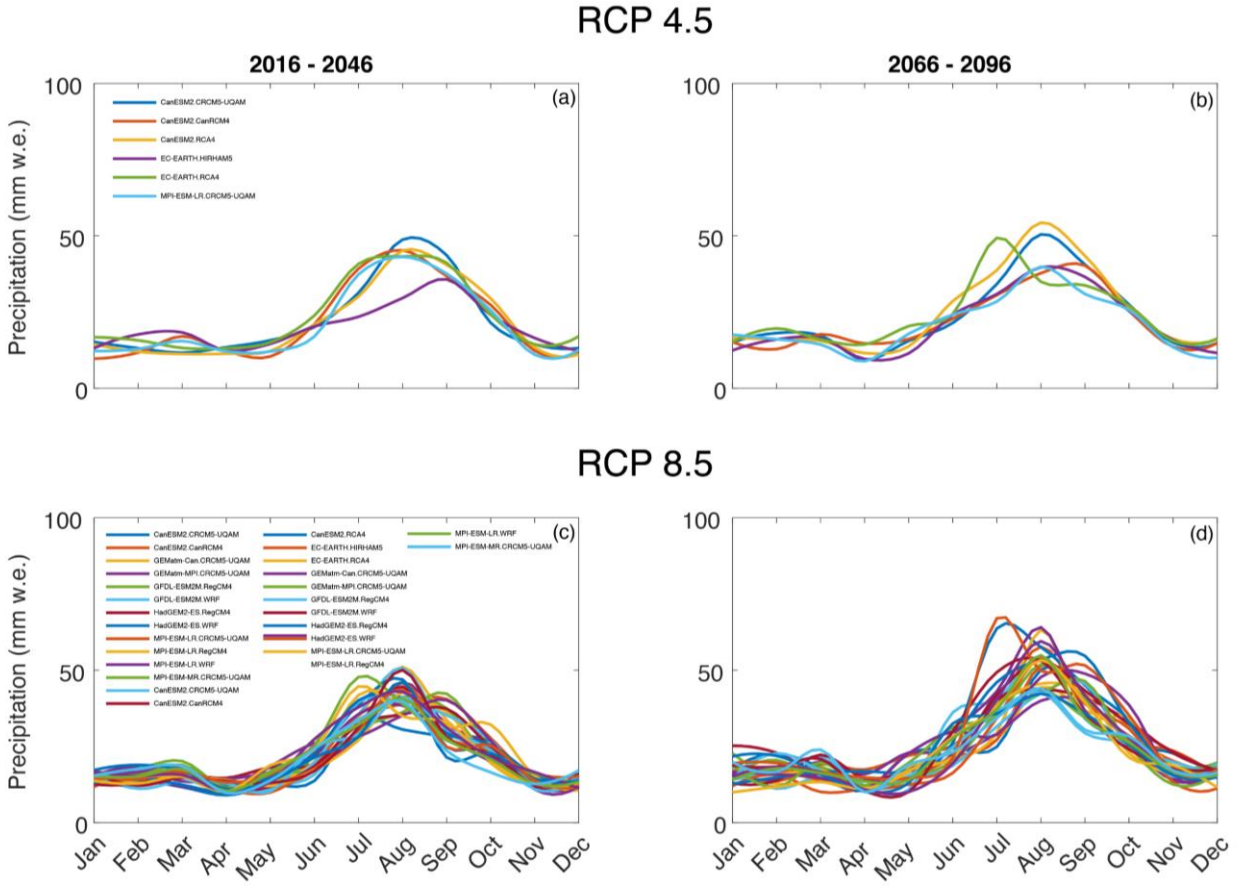

APPENDIX A1 – NA-CORDEX ensemble median monthly precipitation (Jan – Dec) split by individual ensemble member (RCP 4.5 n=6, RCP 8.5 n=27).

APPENDIX B – Zero curtain duration

CLM5.0 simulations indicate minimal changes in late winter zero-curtain duration but a notable increase in early winter zero-curtain duration. The early winter has been identified as a key period in facilitating carbon emissions from Arctic tundra, particularly methane (Tao et al., 2021). Variation in future zero-curtain duration from August to December is presented below.

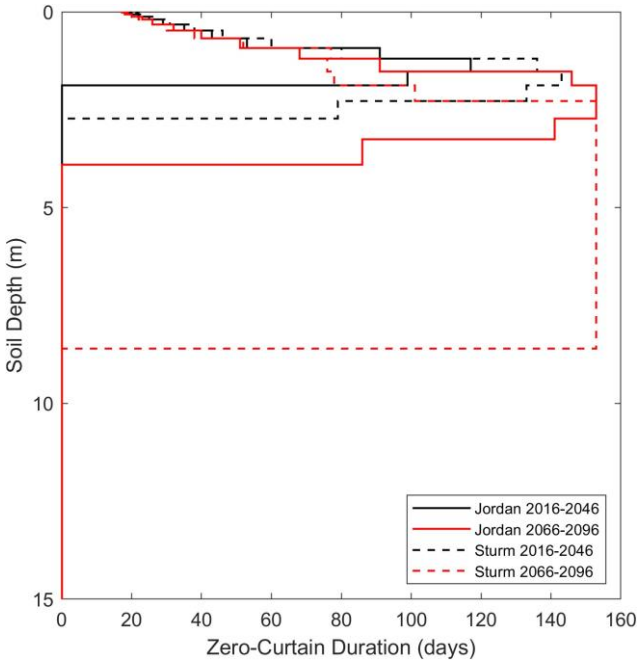

APPENDIX B1 – Aug-Dec zero-curtain duration with soil depth for CORDEX-Jordan (solid black and red lines) and CORDEX-Sturm (dashed black and red lines) for 2016-2046 and 2066-2096.

To further constrain CLM5.0 parameter uncertainties values of Ψ_{min} and Q10 were adjusted alongside two parameterisations for K_{eff} (Jordan and Sturm). A range of realistic Ψ_{min} and Q10 values were chosen as per Dutch et al. (2023) alongside a range of Q10ch4.

APPENDIX C – CLM5.0 parameter assessment space

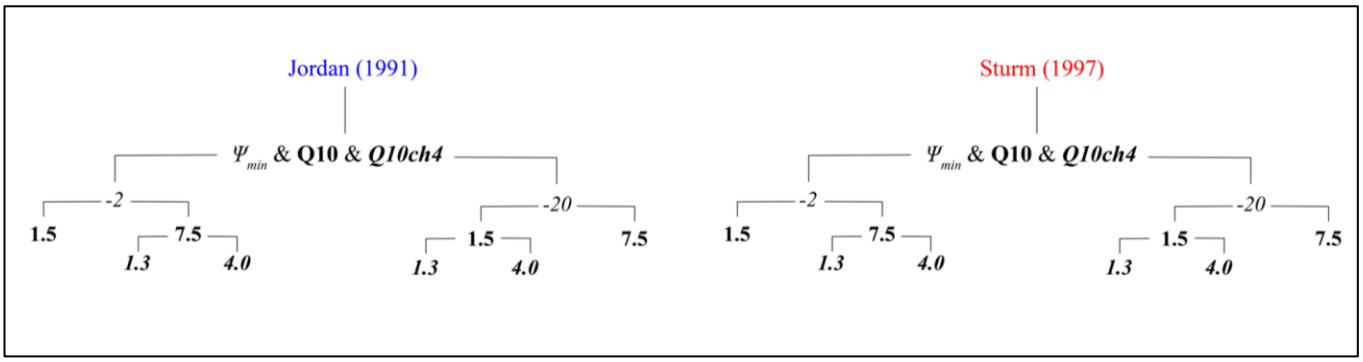

APPENDIX C1 – Schematic showing the range of Q10 (light blue) and Ψ_{min} (green) values applied to CLM5.0 using CORDEX-Jordan (blue) and CORDEX-Sturm (red) for the modelling experiment.

The full combination of applying changes in K_{eff}, Ψ_{min}, Q10 and Q10ch4 as well as the variability provided by the CORDEX ensemble is presented in the main document. The below figure shows the upper and lower bounds of simulated CO_2 and CH_4 when parameter adjustments are applied, with Q10=7.5, Ψ_{min} = -2, Q10ch4 = 4.0 being the lower extreme and Q10=1.5, Ψ_{min} = -20, Q10ch4 = 1.3 being the upper extreme.

APPENDIX D – Cumulative soil carbon emissions as constrained by 'snow-down' and irrespective of snow

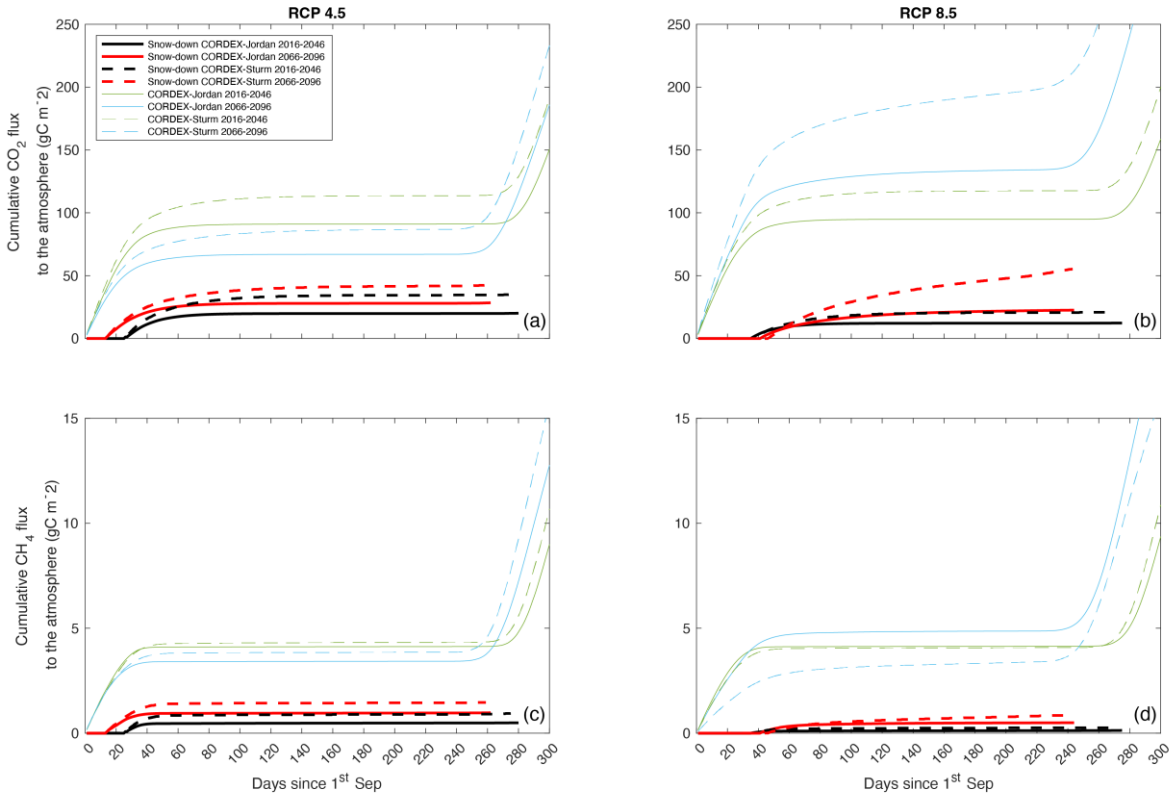

APPENDIX D1 – CLM5.0 simulated cumulative CO_2 and CH_4 flux to the atmosphere constrained by the snow-down period (red, black) and irrespective of snow (green, blue) over two 30-year time periods: 2016-2046 (black, green) and 2066-2096 (red, blue) under RCP 4.5 and RCP 8.5, for TVC using meteorological forcing from an ensemble of 33 RCM-GCM combinations (RC P 4.5 n=6, RCP 8.5 n=27). Solid lines show median values from CORDEX-Jordan ensemble and dashed lines show values for the CORDEX-Sturm ensemble. Variable plot line lengths are indicative of changes in snow-season length.

APPENDIX E – Cumulative soil carbon emissions as constrained by 'snow-down' and irrespective of snow

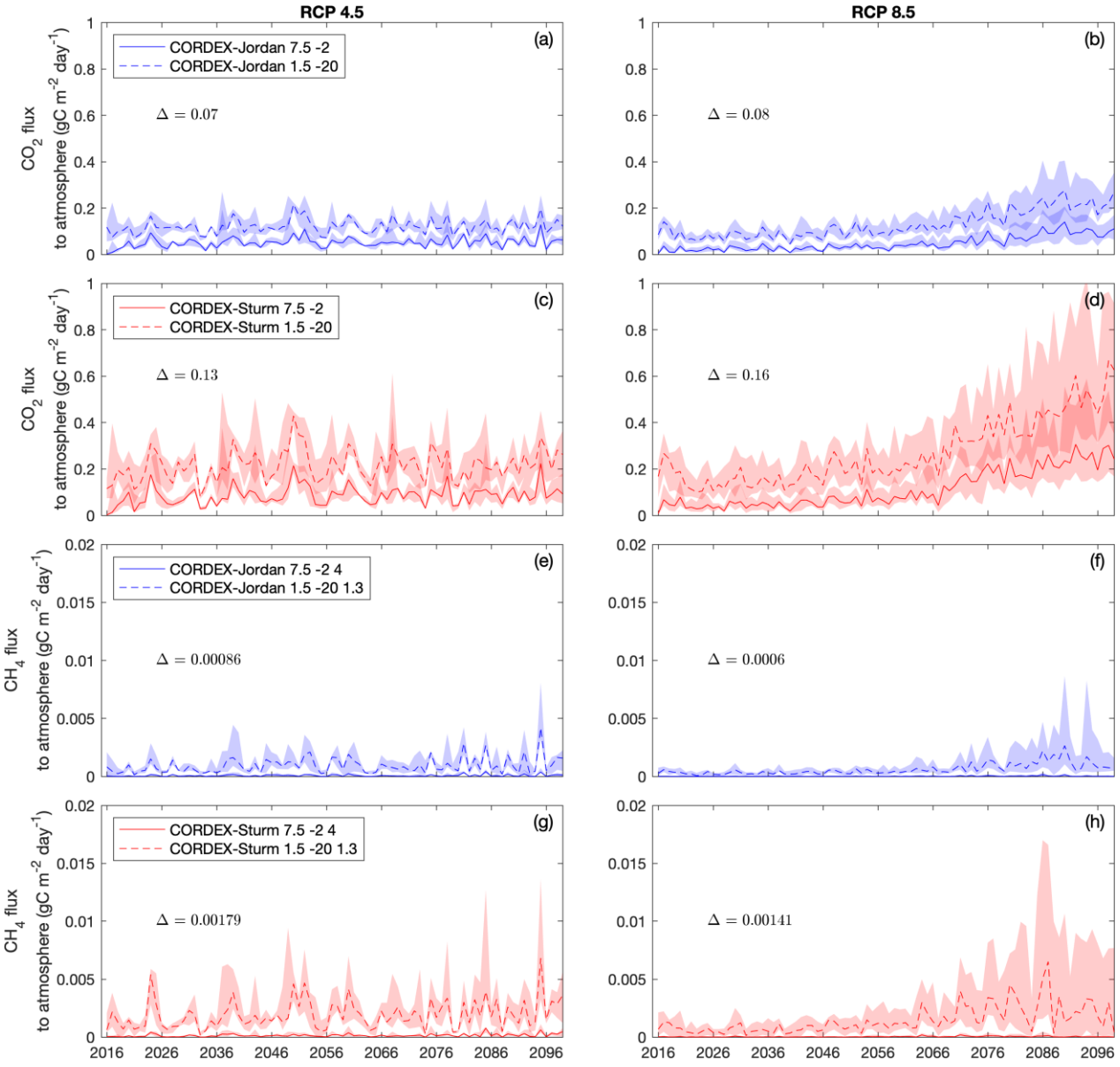

APPENDIX E1 – CLM5.0 simulated median soil respiration for the winter season, comparing the CORDEX-Jordan (blue) ensemble with CORDEX-Sturm (red) for two RCP scenarios (RCP 4.5 n=6, RCP 8.5 n=27). Shaded areas represent 75th and 25th percentiles and represent the CORDEX ensemble distribution. Each plot shows the extremes of Q10, Ψ_{min} and Q10ch4 from the chosen parameter values seen in Appendix C1, where the lower end Ψ_{min} = -2, Q10 = 7.5, Q10ch4 = 4 supresses carbon output to and upper end Ψ_{min} = -20, Q10 = 1.5, Q10ch4 = 1.3 which stimulates carbon output. The average difference between the displayed parameters (solid versus dashed lines, Δ) is included on each subplot.

Appendix F – Frequency distribution of precipitation events in March, June, August and September 2016-2100

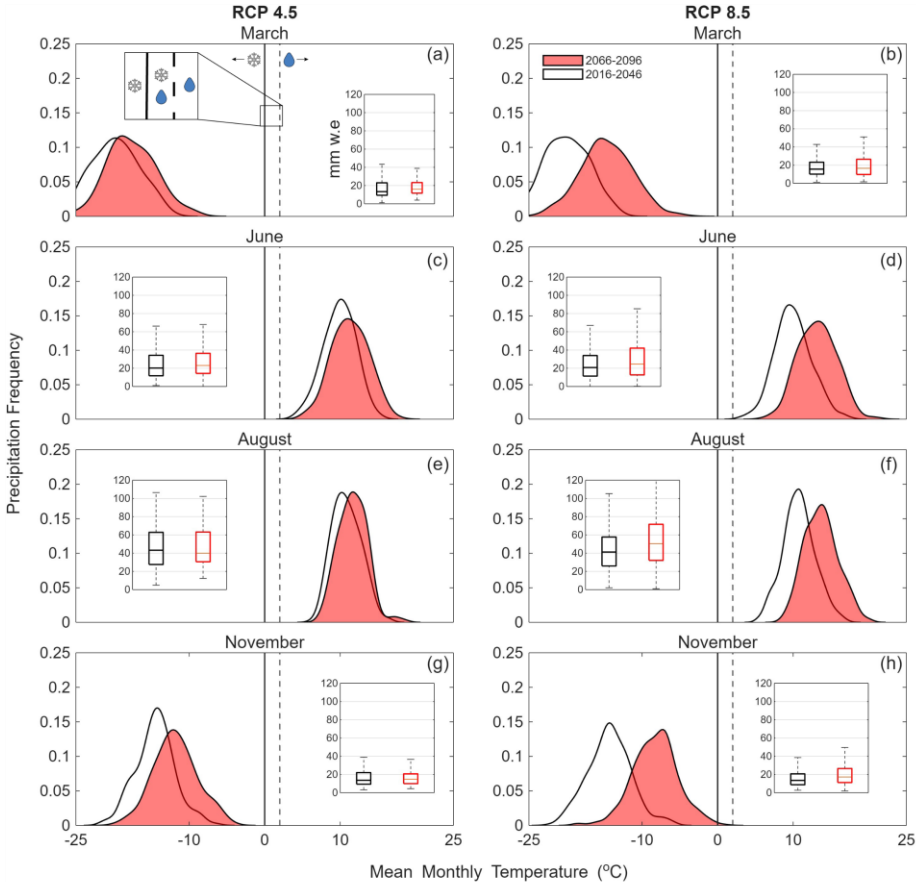

APPENDIX F1 – Half-violin plots show the frequency distribution of precipitation events as a function of air temperature for TVC in March, June, August and November under RCP 4.5 (left) and RCP 8.5 (right) over two 30-year time periods: from an ensemble of 33 NA-CORDEX GCM-GCM combinations (RCP 4.5 n=6, RCP 8.5 n=27). White violins with black outlines represent 2016-2046 (black) and red violins 2066-2096. (red) under RCP 4.5 and RCP 8.5, for TVC using meteorological data from an ensemble of 33 NA-CORDEX GCM-GCM combinations (RCP 4.5 n=6, RCP 8.5 n=27). The height of each violin represents the frequency of precipitation events at a given temperature. The solid and dashed black lines at 0 and 2 °C show transitional temperatures between snow and rain where CLM5.0 treats the transition in precipitation phase as a linear ramp. Inset boxplots show monthly total precipitation for the two 30-year periods.

Code and Data Availability

Code and data to produce figures is available at: https://github.com/Jruthers/paper1/

Author Contribution

Experimental Design, CORDEX Bias Correction, CLM5.0 Simulations, Analysis and Draft preparation; JR, NR, LW, AC. Supervision; NR, LW. All authors were involved in reviewing and editing prior to submission.

Competing Interests

The authors declare no competing interests.

Acknowledgements

JR was funded by a Research and Development Fund (RDF) Studentship from Northumbria University. The work was supported by a National Environmental Research Council (NERC) Seedcorn grant awarded to NR and LW; Carbon Emissions Under Arctic Snow (CEAS) project reference: NE/W003686/1. The authors thank R. Tutton, P. Marsh, R. Essery, R. Thorne, G. Hould Gosselin, B. Walker, O. Sonnentag, J. Griffith, and B. Darkin, for providing the field measurements required for CORDEX bias correction and thanks to Oliver Sonnentag and Bo Qu for advice on the approaches to process and bias correct CORDEX data. The authors thank C. Derksen, and G. Hould Gosselin for providing comments and edits to this manuscript. A raincloud plot function written by www.tomrmarshall.com was used to create the precipitation frequency plots shown in Figure 2.

References

Aalto, J., Karjalainen, O., Hjort, J. & Luoto, M. 2018. Statistical forecasting of current and future circum-arctic ground temperatures and active layer thickness. *Geophysical Research Letters,* 45**,** 4889-4898.

Amap, A. M. a. a. P. 2017. Snow, water, ice and permafrost in the arctic (swipa) 2017.

Andren, O. & Paustian, K. 1987. Barley straw decomposition in the field: A comparison of models. *Ecology,* 68**,** 1190-1200.

Arndt, K. A., Lipson, D. A., Hashemi, J., Oechel, W. C. & Zona, D. 2020. Snow melt stimulates ecosystem respiration in arctic ecosystems. *Global Change Biology,* 26**,** 5042-5051.

Bigalke, S. & Walsh, J. E. 2022. Future changes of snow in alaska and the arctic under stabilized global warming scenarios. *Atmosphere,* 13**,** 541.

Bintanja, R. & Andry, O. 2017. Towards a rain-dominated arctic. *Nature Climate Change,* 7**,** 263-267.

Bliss, L. & Matveyeva, N. 1992. Circumpolar arctic vegetation. *Arctic ecosystems in a changing climate: an ecophysiological perspective,* 59**,** 89.

Callaghan, T. V., Johansson, M., Brown, R. D., Groisman, P. Y., Labba, N., Radionov, V., Bradley, R. S., Blangy, S., Bulygina, O. N., Christensen, T. R., Colman, J. E., Essery, R. L. H., Forbes, B. C., Forchhammer, M. C., Golubev, V. N., Honrath, R. E., Juday, G. P., Meshcherskaya, A. V., Phoenix, G. K., Pomeroy, J., Rautio, A., Robinson, D. A., Schmidt, N. M., Serreze, M. C., Shevchenko, V. P., Shiklomanov, A. I., Shmakin, A. B., Sköld, P., Sturm, M., Woo, M.-K. & Wood, E. F. 2011. Multiple effects of changes in arctic snow cover. *AMBIO,* 40**,** 32-45.

Cannon, A. J. 2018. Multivariate quantile mapping bias correction: An n-dimensional probability density function transform for climate model simulations of multiple variables. *Climate dynamics,* 50**,** 31-49.

Cannon, A. J., Alford, H., Shrestha, R. R., Kirchmeier-Young, M. C. & Najafi, M. R. 2022. Canadian large ensembles adjusted dataset version 1 (canleadv1): Multivariate bias-corrected climate model outputs for terrestrial modelling and attribution studies in north america. Wiley Online Library.

Chen, S., Wang, J., Zhang, T. & Hu, Z. 2020. Climatic, soil, and vegetation controls of the temperature sensitivity (q10) of soil respiration across terrestrial biomes. *Global Ecology and Conservation,* 22**,** e00955.

Christensen, J. H., Kanikicharla, K. K., Aldrian, E., An, S. I., Cavalcanti, I. F. A., De Castro, M., Dong, W., Goswami, P., Hall, A. & Kanyanga, J. K. 2013. Climate phenomena and their relevance for future regional climate change. *Climate change 2013 the physical science basis: Working group i contribution to the fifth assessment report of the intergovernmental panel on climate change.* Cambridge University Press.

Cohen, J., Ye, H. & Jones, J. 2015. Trends and variability in rain-on-snow events. *Geophysical Research Letters,* 42**,** 7115-7122.

Commane, R., Lindaas, J., Benmergui, J., Luus, K. A., Chang, R. Y.-W., Daube, B. C., Euskirchen, E. S., Henderson, J. M., Karion, A. & Miller, J. B. 2017. Carbon dioxide sources from alaska driven by increasing early winter respiration from arctic tundra. *Proceedings of the National Academy of Sciences,* 114**,** 5361-5366.

Dutch, V. R., Rutter, N., Wake, L., Sandells, M., Derksen, C., Walker, B., Hould Gosselin, G., Sonnentag, O., Essery, R. & Kelly, R. 2021. Impact of measured and simulated tundra snowpack properties on heat transfer. *The Cryosphere Discussions***,** 1-24.

Dutch, V. R., Rutter, N., Wake, L., Sonnentag, O., Hould Gosselin, G., Sandells, M., Derksen, C., Walker, B., Meyer, G., Essery, R., Kelly, R., Marsh, P., Boike, J. & Detto, M. 2023. Simulating net ecosystem exchange under seasonal snow cover at an arctic tundra site. Copernicus GmbH.

Ednie, M. & Smith, S. 2015. Permafrost temperature data 2008–2014 from community based monitoring sites in nunavut. *Geological Survey of Canada Open File,* 7784.

Elberling, B. & Brandt, K. K. 2003. Uncoupling of microbial co2 production and release in frozen soil and its implications for field studies of arctic c cycling. *Soil Biology and Biochemistry,* 35**,** 263-272.

Euskirchen, E., Bret-Harte, M., Shaver, G., Edgar, C. & Romanovsky, V. 2017. Long-term release of carbon dioxide from arctic tundra ecosystems in alaska. *Ecosystems,* 20**,** 960-974.

Fahnestock, J. T., Jones, M. H. & Welker, J. M. 1999. Wintertime co2 efflux from arctic soils: Implications for annual carbon budgets. *Global Biogeochemical Cycles,* 13**,** 775-779.

Fierer, N., Craine, J. M., Mclauchlan, K. & Schimel, J. P. 2005. Litter quality and the temperature sensitivity of decomposition. *Ecology,* 86**,** 320-326.

Grünberg, I., Cable, B., Antonova, S., Lange, S. & Boike, J. Soil temperature and thaw depth differences associated with tundra vegetation types at trail valley creek, nwt, canada. 2019.

Harr, R. D. 1981. Some characteristics and consequences of snowmelt during rainfall in western oregon. *Journal of Hydrology,* 53**,** 277-304.

Hugelius, G., Strauss, J., Zubrzycki, S., Harden, J. W., Schuur, E., Ping, C.-L., Schirrmeister, L., Grosse, G., Michaelson, G. J. & Koven, C. D. 2014. Estimated stocks of circumpolar permafrost carbon with quantified uncertainty ranges and identified data gaps. *Biogeosciences,* 11**,** 6573-6593.

Intergovernmental Panel on Climate, C. 2023. *Climate change 2022 – impacts, adaptation and vulnerability: Working group ii contribution to the sixth assessment report of the intergovernmental panel on climate change,* Cambridge, Cambridge University Press.

Ito, A., Li, T., Qin, Z., Melton, J., Tian, H., Kleinen, T., Zhang, W., Zhang, Z., Joos, F. & Ciais, P. 2023. Cold-season methane fluxes simulated by gcp-ch4 models. *Geophysical Research Letters,* 50**,** e2023GL103037.

Jordan, R. E. 1991. A one-dimensional temperature model for a snow cover: Technical documentation for sntherm. 89.

King, J., Derksen, C., Toose, P., Langlois, A., Larsen, C., Lemmetyinen, J., Marsh, P., Montpetit, B., Roy, A. & Rutter, N. 2018. The influence of snow microstructure on dual-frequency radar measurements in a tundra environment. *Remote sensing of environment,* 215**,** 242-254.

Kittler, F., Heimann, M., Kolle, O., Zimov, N., Zimov, S. & Göckede, M. 2017. Long-term drainage reduces co2 uptake and ch4 emissions in a siberian permafrost ecosystem. *Global Biogeochemical Cycles,* 31**,** 1704-1717.

Koven, C. D., Riley, W. J. & Stern, A. 2013. Analysis of permafrost thermal dynamics and response to climate change in the cmip5 earth system models. *Journal of Climate,* 26**,** 1877-1900.

Larson, E. J., Schiferl, L. D., Commane, R., Munger, J. W., Trugman, A. T., Ise, T., Euskirchen, E. S., Wofsy, S. & Moorcroft, P. M. 2021. The changing carbon balance of tundra ecosystems: Results from a vertically-resolved peatland biosphere model. *Environmental Research Letters,* 17**,** 014019.

Lawrence, D. M., Fisher, R. A., Koven, C. D., Oleson, K. W., Swenson, S. C., Bonan, G., Collier, N., Ghimire, B., Van Kampenhout, L. & Kennedy, D. 2019. The community land model version 5: Description of new features, benchmarking, and impact of forcing uncertainty. *Journal of Advances in Modeling Earth Systems,* 11**,** 4245-4287.

Lawrence, D. M., Koven, C. D., Swenson, S. C., Riley, W. J. & Slater, A. 2015. Permafrost thaw and resulting soil moisture changes regulate projected high-latitude co2 and ch4 emissions. *Environmental Research Letters,* 10**,** 094011.

Marsh, P., Onclin, C. & Neumann, N. 2002. Water and energy fluxes in the lower mackenzie valley, 1994/95. *Atmosphere-Ocean,* 40**,** 245-256.

Marshall, H., Conway, H. & Rasmussen, L. 1999. Snow densification during rain. *Cold Regions Science and Technology,* 30**,** 35-41.

Mastepanov, M., Sigsgaard, C., Tagesson, T., Ström, L., Tamstorf, M., Lund, M. & Christensen, T. 2013. Revisiting factors controlling methane emissions from high-arctic tundra. *Biogeosciences,* 10**,** 5139-5158.

Mazurkiewicz, A. B., Callery, D. G. & Mcdonnell, J. J. 2008. Assessing the controls of the snow energy balance and water available for runoff in a rain-on-snow environment. *Journal of Hydrology,* 354**,** 1-14.

Mccrystall, M. R., Stroeve, J., Serreze, M., Forbes, B. C. & Screen, J. A. 2021. New climate models reveal faster and larger increases in arctic precipitation than previously projected. *Nat Commun,* 12**,** 6765.

Mcginnis, S. & Mearns, L. 2021. Building a climate service for north america based on the na-cordex data archive. *Climate Services,* 22**,** 100233.

Miner, K. R., Turetsky, M. R., Malina, E., Bartsch, A., Tamminen, J., Mcguire, A. D., Fix, A., Sweeney, C., Elder, C. D. & Miller, C. E. 2022. Permafrost carbon emissions in a changing arctic. *Nature Reviews Earth & Environment,* 3**,** 55-67.

Mudryk, L., Brown, R., Derksen, C., Luojus, K., Decharme, B. & Helfrich, S. 2019. Terrestrial snow cover. Arctic Program Alexandria, VA, USA.

Mudryk, L., Santolaria-Otín, M., Krinner, G., Ménégoz, M., Derksen, C., Brutel-Vuilmet, C., Brady, M. & Essery, R. 2020. Historical northern hemisphere snow cover trends and projected changes in the cmip6 multi-model ensemble. *The Cryosphere,* 14**,** 2495-2514.

Müller, J., Paudel, R., Shoemaker, C., Woodbury, J., Wang, Y. & Mahowald, N. 2015. Ch 4 parameter estimation in clm4. 5bgc using surrogate global optimization. *Geoscientific Model Development,* 8**,** 3285-3310.

Natali, S. M., Watts, J. D., Rogers, B. M., Potter, S., Ludwig, S. M., Selbmann, A.-K., Sullivan, P. F., Abbott, B. W., Arndt, K. A. & Birch, L. 2019. Large loss of co2 in winter observed across the northern permafrost region. *Nature Climate Change,* 9**,** 852-857.

Pedron, S., Jespersen, R., Xu, X., Khazindar, Y., Welker, J. & Czimczik, C. 2023. More snow accelerates legacy carbon emissions from arctic permafrost. *AGU Advances,* 4**,** e2023AV000942.

Pongracz, A., Wårlind, D., Miller, P. A. & Parmentier, F.-J. W. 2021. Model simulations of arctic biogeochemistry and permafrost extent are highly sensitive to the implemented snow scheme in lpj-guess. *Biogeosciences,* 18**,** 5767-5787.

Quinton, W., Gray, D. & Marsh, P. 2000. Subsurface drainage from hummock-covered hillslopes in the arctic tundra. *Journal of Hydrology,* 237**,** 113-125.

Raz-Yaseef, N., Torn, M. S., Wu, Y., Billesbach, D. P., Liljedahl, A. K., Kneafsey, T. J., Romanovsky, V. E., Cook, D. R. & Wullschleger, S. D. 2017. Large co2 and ch4 emissions from polygonal tundra during spring thaw in northern alaska. *Geophysical Research Letters,* 44**,** 504-513.

Riley, W., Subin, Z., Lawrence, D., Swenson, S., Torn, M., Meng, L., Mahowald, N. & Hess, P. 2011. Barriers to predicting changes in global terrestrial methane fluxes: Analyses using clm4me, a methane biogeochemistry model integrated in cesm. *Biogeosciences,* 8**,** 1925-1953.

Royer, A., Picard, G., Vargel, C., Langlois, A., Gouttevin, I. & Dumont, M. 2021. Improved simulation of arctic circumpolar land area snow properties and soil temperatures. *Frontiers in Earth Science,* 9**,** 515.

Schaefer, K. & Jafarov, E. 2015. A parameterization of respiration in frozen soils based on substrate availability. *Biogeosciences Discussions,* 12.

Schimel, J. P., Bilbrough, C. & Welker, J. M. 2004. Increased snow depth affects microbial activity and nitrogen mineralization in two arctic tundra communities. *Soil Biology and Biochemistry,* 36**,** 217-227.

Schimel, J. P., Fahnestock, J., Michaelson, G., Mikan, C., Ping, C.-L., Romanovsky, V. E. & Welker, J. 2006. Cold-season production of co2 in arctic soils: Can laboratory and field estimates be reconciled through a simple modeling approach? *Arctic, Antarctic, and Alpine Research,* 38**,** 249-256.

Schuur, E. A., Mcguire, A. D., Schädel, C., Grosse, G., Harden, J. W., Hayes, D. J., Hugelius, G., Koven, C. D., Kuhry, P. & Lawrence, D. M. 2015. Climate change and the permafrost carbon feedback. *Nature,* 520**,** 171-179.

Serreze, M. C., Gustafson, J., Barrett, A. P., Druckenmiller, M. L., Fox, S., Voveris, J., Stroeve, J., Sheffield, B., Forbes, B. C. & Rasmus, S. 2021. Arctic rain on snow events: Bridging observations to understand environmental and livelihood impacts. *Environmental Research Letters,* 16**,** 105009.

Shogren, A. J., Zarnetske, J. P., Abbott, B. W., Iannucci, F. & Bowden, W. B. 2020. We cannot shrug off the shoulder seasons: Addressing knowledge and data gaps in an arctic headwater. *Environmental Research Letters,* 15**,** 104027.

Sturm, M., Holmgren, J., König, M. & Morris, K. 1997. The thermal conductivity of seasonal snow. *Journal of Glaciology,* 43**,** 26-41.

Sturtevant, C., Oechel, W., Zona, D. & Emerson, C. 2011. Soil moisture control over autumn season methane flux, arctic coastal plain of alaska. *Biogeosciences Discussions,* 8.

Sturtevant, C., Oechel, W., Zona, D., Kim, Y. & Emerson, C. 2012. Soil moisture control over autumn season methane flux, arctic coastal plain of alaska. *Biogeosciences,* 9**,** 1423-1440.

Tao, J., Zhu, Q., Riley, W. J. & Neumann, R. B. 2021. Improved elmv1-eca simulations of zero-curtain periods and cold-season ch 4 and co 2 emissions at alaskan arctic tundra sites. *The Cryosphere,* 15**,** 5281-5307.

Thompson, A., Kelly, R. & Marsh, P. Spatial variability of snow at trail valley creek, nwt. 73rd Eastern Snow Conference, Columbus, Ohio, USA, 2016. 101-108.

Treat, C. C., Virkkala, A. M., Burke, E., Bruhwiler, L., Chatterjee, A., Fisher, J. B., Hashemi, J., Parmentier, F. J. W., Rogers, B. M. & Westermann, S. 2024. Permafrost carbon: Progress on understanding stocks and fluxes across northern terrestrial ecosystems. *Journal of Geophysical Research: Biogeosciences,* 129**,** e2023JG007638.

Trenberth, K. E. 1998. Atmospheric moisture residence times and cycling: Implications for rainfall rates and climate change. *Climatic change,* 39**,** 667-694.

Tutton, R., Darkin, B., Essery, R., Griffith, J., Hould Gosselin, G., Marsh, P., Sonnentag, O., Thorne, R., and Walker, B. 2024. A 885 hydro-meterological dataset from the taiga-tundra ecotone in the western canadian arctic: Trail valley creek, northwest territories.

Voigt, C., Virkkala, A.-M., Hould Gosselin, G., Bennett, K. A., Black, T. A., Detto, M., Chevrier-Dion, C., Guggenberger, G., Hashmi, W. & Kohl, L. 2023. Arctic soil methane sink increases with drier conditions and higher ecosystem respiration. *Nature climate change,* 13**,** 1095-1104.

Webb, E. E., Schuur, E. A., Natali, S. M., Oken, K. L., Bracho, R., Krapek, J. P., Risk, D. & Nickerson, N. R. 2016. Increased wintertime co2 loss as a result of sustained tundra warming. *Journal of Geophysical Research: Biogeosciences,* 121**,** 249-265.

Welker, J., Fahnestock, J. & Jones, M. 2000. Annual co2 flux in dry and moist arctic tundra: Field responses to increases in summer temperatures and winter snow depth. *Climatic Change,* 44**,** 139-150.

Wilcox, E. J., Keim, D., De Jong, T., Walker, B., Sonnentag, O., Sniderhan, A. E., Mann, P. & Marsh, P. 2019. Tundra shrub expansion may amplify permafrost thaw by advancing snowmelt timing. *Arctic Science,* 5**,** 202-217.

Yan, D., Li, J., Pei, J., Cui, J., Nie, M. & Fang, C. 2017. The temperature sensitivity of soil organic carbon decomposition is greater in subsoil than in topsoil during laboratory incubation. *Scientific reports,* 7**,** 5181.

Zhang, T. 2005. Influence of the seasonal snow cover on the ground thermal regime: An overview. *Reviews of geophysics (1985),* 43**,** RG4002-n/a.

Zona, D., Gioli, B., Commane, R., Lindaas, J., Wofsy, S. C., Miller, C. E., Dinardo, S. J., Dengel, S., Sweeney, C. & Karion, A. 2016. Cold season emissions dominate the arctic tundra methane budget. *Proceedings of the National Academy of Sciences,* 113**,** 40-45.